

NASA/TM-2002-211737



Mixed-Mode Decohesion Finite Elements for the Simulation of Delamination in Composite Materials

Pedro P. Camanho
University of Porto, Porto, Portugal

Carlos G. Dávila
Langley Research Center, Hampton, Virginia

June 2002

The NASA STI Program Office ... in Profile

Since its founding, NASA has been dedicated to the advancement of aeronautics and space science. The NASA Scientific and Technical Information (STI) Program Office plays a key part in helping NASA maintain this important role.

The NASA STI Program Office is operated by Langley Research Center, the lead center for NASA's scientific and technical information. The NASA STI Program Office provides access to the NASA STI Database, the largest collection of aeronautical and space science STI in the world. The Program Office is also NASA's institutional mechanism for disseminating the results of its research and development activities. These results are published by NASA in the NASA STI Report Series, which includes the following report types:

- **TECHNICAL PUBLICATION.** Reports of completed research or a major significant phase of research that present the results of NASA programs and include extensive data or theoretical analysis. Includes compilations of significant scientific and technical data and information deemed to be of continuing reference value. NASA counterpart of peer-reviewed formal professional papers, but having less stringent limitations on manuscript length and extent of graphic presentations.
- **TECHNICAL MEMORANDUM.** Scientific and technical findings that are preliminary or of specialized interest, e.g., quick release reports, working papers, and bibliographies that contain minimal annotation. Does not contain extensive analysis.
- **CONTRACTOR REPORT.** Scientific and technical findings by NASA-sponsored contractors and grantees.
- **CONFERENCE PUBLICATION.** Collected papers from scientific and technical conferences, symposia, seminars, or other meetings sponsored or co-sponsored by NASA.
- **SPECIAL PUBLICATION.** Scientific, technical, or historical information from NASA programs, projects, and missions, often concerned with subjects having substantial public interest.
- **TECHNICAL TRANSLATION.** English-language translations of foreign scientific and technical material pertinent to NASA's mission.

Specialized services that complement the STI Program Office's diverse offerings include creating custom thesauri, building customized databases, organizing and publishing research results ... even providing videos.

For more information about the NASA STI Program Office, see the following:

- Access the NASA STI Program Home Page at <http://www.sti.nasa.gov>
- E-mail your question via the Internet to help@sti.nasa.gov
- Fax your question to the NASA STI Help Desk at (301) 621-0134
- Phone the NASA STI Help Desk at (301) 621-0390
- Write to:
NASA STI Help Desk
NASA Center for Aerospace Information
7121 Standard Drive
Hanover, MD 21076-1320

NASA/TM-2002-211737



Mixed-Mode Decohesion Finite Elements for the Simulation of Delamination in Composite Materials

Pedro P. Camanho
University of Porto, Porto, Portugal

Carlos G. Dávila
Langley Research Center, Hampton, Virginia

National Aeronautics and
Space Administration

Langley Research Center
Hampton, Virginia 23681-2199

June 2002

Acknowledgments

The authors would like to acknowledge the assistance of those individuals who aided in the preparation of this document. Dr. James Reeder and Dr. Alfredo Balacó de Morais provided the experimental data, and Dr. Pedro Areiras' useful discussions helped in the development of some of the concepts presented here.

Available from:

NASA Center for AeroSpace Information (CASI)
7121 Standard Drive
Hanover, MD 21076-1320
(301) 621-0390

National Technical Information Service (NTIS)
5285 Port Royal Road
Springfield, VA 22161-2171
(703) 605-6000

Mixed-Mode Decohesion Finite Elements for the Simulation of Delamination in Composite Materials

P.P. Camanho* and C.G. Dávila†

Abstract

A new decohesion element with mixed-mode capability is proposed and demonstrated. The element is used at the interface between solid finite elements to model the initiation and non-self-similar growth of delaminations. A single relative displacement-based damage parameter is applied in a softening law to track the damage state of the interface and to prevent the restoration of the cohesive state during unloading. The softening law for mixed-mode delamination propagation can be applied to any mode interaction criterion such as the two-parameter power law or the three-parameter Benzeggagh-Kenane criterion. To demonstrate the accuracy of the predictions and the irreversibility capability of the constitutive law, steady-state delamination growth is simulated for quasi-static loading-unloading cycles of various single mode and mixed-mode delamination test specimens.

1 Introduction

Interlaminar damage (delamination) is one of the predominant forms of failure in many laminated composites systems, especially when there is no reinforcement in the thickness direction. Delamination as a result of impact or a manufacturing defect can cause a significant reduction in the compressive load-carrying capacity of a structure. The stress gradients that occur near geometric discontinuities such

*DEMEGI, Faculdade de Engenharia, Universidade do Porto, Portugal; Visiting Scientist, Mechanics & Durability Branch, NASA Langley Research Center, U.S.A.

†Analytical & Computational Methods Branch, NASA Langley Research Center, U.S.A.

as ply drop-offs, stiffener terminations and flanges, bonded and bolted joints, and access holes promote delamination initiation, trigger intraply damage mechanisms, and may cause a significant loss of structural integrity.

The fracture process in high performance composite laminates is quite complex, involving not only delamination, but also intralaminar damage mechanisms (e.g. transverse matrix cracking, fiber fracture). For effective predictive capabilities, failure analysis tools for the different failure modes are required.

The simulation of delamination in composites is usually divided into delamination initiation and delamination propagation. Delamination initiation analyses are usually based on stresses and use criteria such as the quadratic interaction of the interlaminar stresses in conjunction with a characteristic distance [1],[2]. The characteristic distance is an averaging length that is a function of geometry and material properties, so its determination always require extensive testing.

Most analyses of delamination growth apply a fracture mechanics approach, and evaluate energy release rates G for self-similar delamination growth [3]-[9]. The energy release rates are usually evaluated using the virtual crack closure technique (VCCT) proposed by Rybicki and Kanninen [10]. The VCCT technique is based on Irwin's assumption that when a crack extends by a small amount, the energy released in the process is equal to the work required to close the crack to its original length. The Mode I, Mode II, and Mode III energy release rates, G_I , G_{II} and G_{III} respectively, can then be computed from the nodal forces and displacements obtained from the solution of a finite element model. The approach is computationally effective since the energy release rates can be obtained from only one analysis. Although valuable information concerning the onset and the stability of delamination can be obtained using the VCCT, its use in the simulation of delamination growth may require complex moving mesh techniques to advance the crack front when the local energy release rates reach a critical value [11]. Furthermore, an initial delamination must be defined and, for certain geometries and load cases, the location of the delamination front might be difficult to determine.

The use of decohesion elements placed at the interfaces between laminae can overcome some of the above difficulties. Decohesion elements are based on a Dudgale-Barenblatt cohesive zone approach [12], [13], which can be related to Griffith's theory of fracture when the cohesive zone size is negligible when compared with characteristic dimensions, regardless of the shape of the constitutive equation [14]. These elements use failure criteria that combine aspects of strength-based analysis to predict the onset of the softening process at the interface and Fracture Mechanics to predict delamination propagation. A main advantage of the use of decohesion elements is the capability to predict both onset and propagation

of delamination without previous knowledge of the crack location and propagation direction.

Decohesion elements can be divided into two main groups: continuous interface elements and point decohesion elements. Different types of continuous decohesion elements have been proposed, ranging from zero-thickness volumetric elements connecting solid elements [15], finite-thickness volumetric elements connecting shell elements [16], and line elements [17]-[18]. Point decohesion elements are identical to non-linear spring elements connecting nodes [19], [20]. A common feature of previously developed decohesion elements is the absence of an interaction criterion for the prediction of softening onset under mixed-mode loading and the use of simplified interaction criteria of the energy release rates for the prediction of delamination propagation. However, experimental evidence shows that for some resins (e.g. epoxies) the dependence of the fracture toughness on the mode ratio may not be expressed by a simplified expression [21]. Under mixed-mode loading conditions, the propagation of delamination should be predicted using physically sound criteria.

The objective of the current work is to develop zero-thickness volumetric decohesion elements able to capture delamination onset and growth under mixed-mode loading conditions. A quadratic interaction between the tractions is proposed to predict softening onset. A criterion able to capture the mixed-mode fracture toughness under different mode ratios is used to predict delamination propagation. The capabilities of the proposed formulation are assessed simulating double cantilever beam (DCB), end-notch flexure (ENF) and mixed-mode bending (MMB) test specimens, and comparing the predictions with experimental data.

2 Decohesion element formulation

2.1 Element kinematics

The zero-thickness decohesion elements with 8-nodes (shown in Figure 1) and 18-nodes are proposed to simulate the resin-rich layer connecting the several laminae of a composite laminate. The constitutive equation of zero-thickness decohesion elements is established in terms of *relative displacements* (also called *displacement discontinuities* [22]) and *tractions* across the interface.

The definition of the relative displacements for an element with a general orientation in space is obtained using a procedure based on the work of Ahmad [23] and Beer [24]. The vector defining the relative displacement in global coordinates,

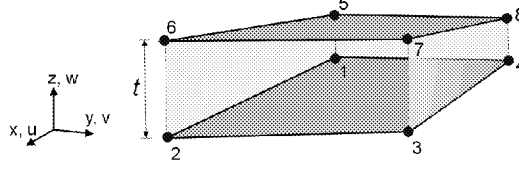


Figure 1: Zero-thickness decohesion element

Δ , can be obtained as:

$$\Delta_i = u_i^+ - u_i^- = N_k u_{ki}^+ - N_k u_{ki}^- = \bar{N}_k u_{ki} \quad (1)$$

where u_{ki}^+ , u_{ki}^- are the displacements in the i direction of the k top and bottom nodes of the element, respectively. N_k are standard Lagrangian shape functions.

For a general element shape and alignment, the normal and tangential relative displacements must be determined in local coordinates. The tangential plane at a given point is spanned by two vectors, \mathbf{v}_ξ and \mathbf{v}_η , obtained by differentiating the global position vector with respect to the natural (local) coordinates:

$$v_{\xi_i} = x_{i,\xi}, \quad v_{\eta_i} = x_{i,\eta} \quad (2)$$

Defining an isoparametric element, the global position vector is obtained as:

$$x_i = N_k x_{ki} \quad (3)$$

From (2) and (3):

$$v_{\xi_i} = (N_k x_{ki})_{,\xi} = N_{k,\xi} x_{ki} \quad (4)$$

$$v_{\eta_i} = (N_k x_{ki})_{,\eta} = N_{k,\eta} x_{ki} \quad (5)$$

Although \mathbf{v}_ξ and \mathbf{v}_η are, generally, not orthogonal to each other, their vector product defines a surface normal. Therefore, the local normal coordinate vector is obtained as:

$$\mathbf{v}_n = (\mathbf{v}_\xi \times \mathbf{v}_\eta) \|\mathbf{v}_\xi \times \mathbf{v}_\eta\|^{-1} \quad (6)$$

The tangential coordinates are then obtained as:

$$\mathbf{v}_s = \mathbf{v}_\xi \|\mathbf{v}_\xi\|^{-1} \quad (7)$$

$$\mathbf{v}_t = \mathbf{v}_n \times \mathbf{v}_s \quad (8)$$

The components of \mathbf{v}_n , \mathbf{v}_s , and \mathbf{v}_t represent the direction cosines of the local coordinate system to the global coordinate system, thus defining the transformation tensor Θ_{si} . Using (1), the relative displacements can then be obtained in local coordinates as:

$$\delta_s = \Theta_{si}\Delta_i = \Theta_{si}\bar{N}_k u_{ki} = B_{sik}u_{ki} \quad (9)$$

The constitutive operator of the decohesion element, D_{sr} , relates the element tractions, τ_s , to the element relative displacements, δ_r :

$$\tau_s = \bar{\delta}_{sr} D_{sr} \delta_r \quad (10)$$

where $\bar{\delta}_{sr}$ is the Kronecker delta.

The coefficients D_{sr} of the element constitutive operator can be used to simulate elaborate mechanical behaviors, including the mechanics of interfacial decohesion and crack propagation, and will be discussed later¹. An important characteristic of the proposed method is that, unlike thin continuum elements (degenerate continuum elements), the stiffness of the interface before softening onset, referred here as the *penalty stiffness*, is not a function of the discretization, but is defined by the coefficients D_{sr} . Some authors [25] have proposed the definition of the penalty stiffness as a function of the interface thickness, t , and elastic moduli of the interface (E_3 , G_{13} and G_{23}) as: $D_{33} = E_3/t$, $D_{11} = 2G_{13}/t$, $D_{22} = 2G_{23}/t$.

The decohesion element stiffness matrix and internal load vector can be obtained from the principle of virtual work:

$$\int_{\Gamma} d\delta_s \tau_s d\Gamma - f_{ki} du_{ki} = 0 \quad (11)$$

From (9), and considering a geometrically linear problem:

$$\int_{\Gamma} B_{sik} \tau_s d\Gamma - f_{ki} = 0 \quad (12)$$

The first term of (12) represents the decohesion element internal load vector. From (9) and (10):

$$\int_{\Gamma} B_{sik} \bar{\delta}_{sr} D_{sr} B_{rvz} d\Gamma u_{zv} = f_{ki} \quad (13)$$

$$K_{ikvz} u_{zv} = f_{ki} \quad (14)$$

¹For simple contact elements D_{sr} are the penalty parameters: $D_{sr} = 0$ if $\delta_3 > 0$, and $D_{33} = K$ if $\delta_3 \leq 0$.

The decohesion element stiffness matrix is then:

$$K_{ikzv} = \int_{\Gamma} B_{sik} \bar{\delta}_{sr} D_{sr} B_{rvz} d\Gamma = \int_{-1}^{+1} \int_{-1}^{+1} B_{sik} \bar{\delta}_{sr} D_{sr} B_{rvz} \|\mathbf{v}_{\xi} \times \mathbf{v}_{\eta}\| d\xi d\eta \quad (15)$$

Care must be exercised in the choice of the integration scheme used to obtain the stiffness matrix and the nodal force vector. Several investigations have shown the superiority of using Newton-Cotes integration techniques over traditional Gaussian integration techniques in decohesion elements [26]-[30]. Using eigenmode analysis of the element stiffness matrices it has been shown that Gaussian integration can cause undesired spurious oscillations of the traction field when large traction gradients are present over an element [28], [29].

Another relevant issue related with the integration scheme is the number of integration points used. Analyses of problems involving crack propagation and softening behavior have shown that the use of full integration was superior to the use of reduced integration schemes [31]. However, Alfano and Crisfield [32] have shown that for linear 4-node decohesion elements increasing the number of integration points from 2 (corresponding to full integration) to 20 results in an increase of spurious oscillations in the load-displacement curve and, consequently, in a less robust solution algorithm. For the above reasons, Newton-Cotes full integration is used in the decohesion element proposed here.

2.2 Proposed constitutive equation

2.2.1 Single-mode delamination

The need for an appropriate constitutive equation in the formulation of the decohesion element is fundamental for an accurate simulation of the interlaminar cracking process. It is considered that there is a *process zone* or *cohesive zone* ahead of the delamination tip. Figure 2 represents the cohesive zone in specimens loaded in pure Mode II (Figure 2-a)) and in pure Mode I (Figure 2-b)). Figure 2 also illustrates the constitutive behaviour for pure Mode I, pure Mode II, and pure Mode III loading. The concept of cohesive zone was initially proposed by Barenblatt [13] and using such a concept the singularity at the crack tip is removed.

Physically, the cohesive zone represents the coalescence of crazes in the resin rich layer located at the delamination tip and reflects the way by which the material loses load-carrying capacity [33]. Ungsuwarungsri and Knauss [33] considered that if the size of the process zone is narrow compared to the size of the specimen, a

softening material behavior confined to a thin layer adjacent to the crack plane is a realistic scheme for the simulation of crack growth. Needleman [34] considered that cohesive zone models are particularly attractive when interfacial strengths are relatively weak when compared with the adjoining material, as is the case in composite laminates.

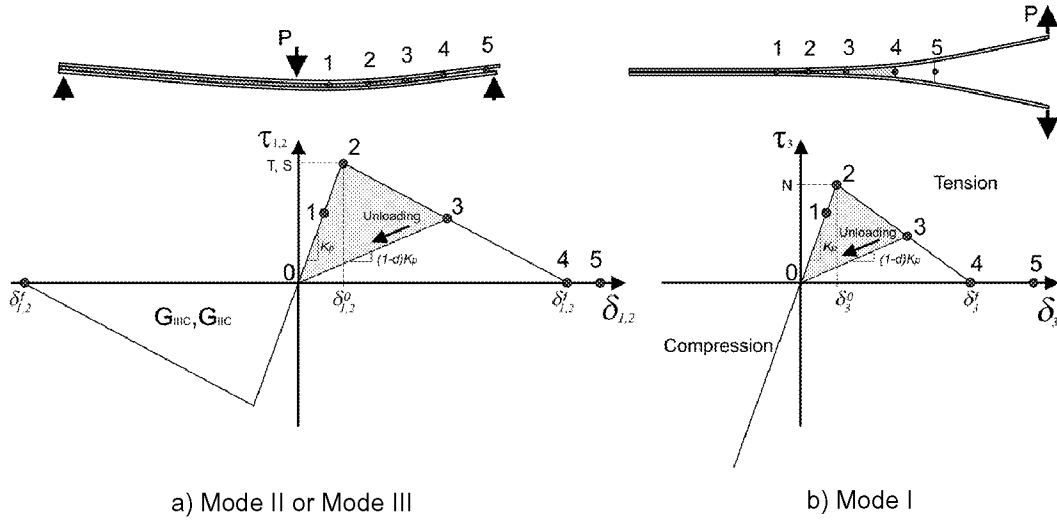


Figure 2: Pure mode constitutive equations

It has been shown that cohesive zone approaches can be related to Griffith's theory of fracture if the area under the traction-relative displacement relation is equal to the corresponding fracture toughness [35] (see Figure 2), regardless of its shape. Furthermore, Crisfield [32] has shown that when the relative displacements δ_3^o and δ_3^f shown in Figure 2 are coincident (corresponding to a sudden load drop to zero) a perfectly brittle fracture is simulated. A model for brittle fracture must be able to capture the high stress gradients at the crack tip with sufficiently fine mesh densities or singular elements.

For pure Mode I and pure Mode II or Mode III loading the bi-linear softening constitutive behaviour represented in Figure 2 is used. A high initial stiffness (*penalty stiffness, K*) is used to hold the top and bottom faces of the decohesion element together in the linear elastic range (point 1 in Figure 2). For pure Mode I, II or III loading, after the interfacial normal or shear tractions attain their respective interlaminar tensile or shear strengths (point 2 in Figure 2), the stiffnesses are

gradually reduced to zero. The onset displacements are obtained as: $\delta_3^o = N/K$, $\delta_2^o = S/K$ and $\delta_1^o = T/K$, where N is the interlaminar tensile strength, and S and T are the interlaminar shear strengths.

The area under the traction-relative displacement curves is the respective (Mode I, II or III) fracture toughness (G_{IC} , G_{IIC} and G_{IIIC} respectively) and defines the final relative displacements, δ_3^f , δ_2^f and δ_1^f , corresponding to complete decohesion:

$$\int_0^{\delta_3^f} \tau_3 d\delta_3 = G_{IC} \quad (16)$$

$$\int_0^{\delta_2^f} \tau_2 d\delta_2 = G_{IIC} \quad (17)$$

$$\int_0^{\delta_1^f} \tau_1 d\delta_1 = G_{IIIC} \quad (18)$$

The final displacements are then obtained as: $\delta_3^f = 2G_{IC}/N$, $\delta_2^f = 2G_{IIC}/S$ and $\delta_1^f = 2G_{IIIC}/T$.

Once a crack is unable to transfer any further load (point 5 in Figure 2), all the penalty stiffnesses revert to zero. However, it is necessary to avoid the interpenetration of the crack faces. The contact problem is addressed by re-applying the normal penalty stiffness when interpenetration is detected.

In order to formulate the complete constitutive equation, the unloading behavior must be defined. It is considered that a softening point unloads towards the origin, as shown in Figure 2. Using the following operator:

$$\langle x \rangle = \begin{cases} 0 & \Leftarrow x \leq 0 \\ x & \Leftarrow x > 0 \end{cases} \quad (19)$$

the loading condition can be formulated in terms of a state variable defined as the *maximum relative displacement*, δ^{\max} , suffered by the point:

$$\text{Mode II or III} : \delta_i^{\max} = \max \{ \delta_i^{\max}, |\delta_i| \}, \quad i = 1, 2 \quad (20)$$

$$\text{Mode I} : \delta_3^{\max} = \max \{ \delta_3^{\max}, \delta_3 \}, \quad \text{with } \delta_3^{\max} \geq 0 \quad (21)$$

and using a *loading function*, F , defined as:

$$\text{Mode II or III} \quad : \quad F(|\delta_i| - \delta_i^{\max}) = \frac{\langle |\delta_i| - \delta_i^{\max} \rangle}{|\delta_i| - \delta_i^{\max}}, i = 1, 2 \quad (22)$$

$$\text{Mode I} \quad : \quad F(\delta_3 - \delta_3^{\max}) = \frac{\langle \delta_3 - \delta_3^{\max} \rangle}{\delta_3 - \delta_3^{\max}}, \quad (23)$$

$$\text{with } \delta_3^{\max} \geq 0.$$

Using δ^{\max} in the constitutive equation, the irreversibility of damage is taken into account. This is shown in Figure 2: if the relative displacement decreases, the point unloads elastically towards the origin with a reduced, secant, stiffness (point 3 in Figure 2).

The irreversible, bi-linear, softening constitutive behaviour shown in Figure 2 have been developed in previous work [17], [32], [36], and can be defined as:

$$\tau_i = \begin{cases} K\delta_i & \Leftarrow \delta_i^{\max} \leq \delta_i^o \\ (1 - d_i)K\delta_i & \Leftarrow \delta_i^o < \delta_i^{\max} < \delta_i^f \\ 0 & \Leftarrow \delta_i^{\max} \geq \delta_i^f \end{cases} \quad (24)$$

$$d_i = \frac{\delta_i^f(\delta_i^{\max} - \delta_i^o)}{\delta_i^{\max}(\delta_i^f - \delta_i^o)}, i = 1, 2, 3; d_i \in [0, 1] \quad (25)$$

In order to avoid interpenetration of the crack faces, the following condition is introduced:

$$\tau_3 = K\delta_3 \Leftarrow \delta_3 \leq 0 \quad (26)$$

The properties required to define the interfacial behavior are the penalty stiffness, K , the corresponding fracture toughness, G_{IC} , G_{IIC} and G_{IIIC} , and the corresponding interlaminar normal tensile or shear strengths, N , S or T respectively.

2.2.2 Mixed-mode delamination

In structural applications of composites, delamination growth is likely to occur under mixed-mode loading. Therefore, a general formulation for decohesion elements dealing with mixed-mode delamination onset and propagation is also required.

Softening onset prediction Under pure Mode I, II or III loading, the onset of damage at the interface can be determined simply by comparing the traction components with their respective allowables. However, under mixed-mode loading damage onset and the corresponding softening behavior may occur before any of the traction components involved reach their respective allowables, which is an issue that is usually neglected in the formulation of decohesion elements. Cui *et al.* [37] have highlighted the importance of the interactions between interlaminar stress components when predicting delamination. It was shown that poor results are obtained using the maximum stress criterion. Therefore, a mixed-mode criterion accounting for the effect of the interaction of the traction components in the onset of delamination is proposed here.

It is assumed that the initiation of the softening process can be predicted using the quadratic failure criterion [37], considering that compressive normal tractions do not affect delamination onset and using the operator defined in (19):

$$\left(\frac{\langle\tau_3\rangle}{N}\right)^2 + \left(\frac{\tau_2}{S}\right)^2 + \left(\frac{\tau_1}{T}\right)^2 = 1 \quad (27)$$

This criterion has been successfully used to predict the onset of delamination in previous investigations [1], [2], [37].

The *total mixed-mode relative displacement* δ_m is defined as:

$$\delta_m = \sqrt{\delta_1^2 + \delta_2^2 + \langle\delta_3\rangle^2} = \sqrt{\delta_{shear}^2 + \langle\delta_3\rangle^2} \quad (28)$$

where δ_{shear} represents the norm of the vector defining the tangential relative displacements of the element.

Using the same penalty stiffness in Modes I, II and III, the tractions before softening onset are:

$$\tau_i = K\delta_i, \quad i = 1, 2, 3 \quad (29)$$

Assuming $S = T$, the single-mode relative displacements at softening onset are:

$$\delta_3^o = \frac{N}{K} \quad (30)$$

$$\delta_1^o = \delta_2^o = \delta_{shear}^o = \frac{S}{K} \quad (31)$$

For an opening displacement δ_3 greater than zero, the mode mixity ratio β is defined as:

$$\beta = \frac{\delta_{shear}}{\delta_3} \quad (32)$$

The mixed-mode relative displacement corresponding to the onset of softening, δ_m^o , is obtained by substituting eqs. (28)-(32) into (27) and solving for δ_m , which gives:

$$\delta_m^o = \begin{cases} \delta_3^o \delta_1^o \sqrt{\frac{1 + \beta^2}{(\delta_1^o)^2 + (\beta \delta_3^o)^2}} \Leftarrow \delta_3 > 0 \\ \delta_{shear}^o \Leftarrow \delta_3 \leq 0 \end{cases} \quad (33)$$

Clearly, pure mode loading is a particular case of the proposed formulation, as $\delta_m^o = \delta_3^o$ for $\beta = 0$ (Mode I), and $\delta_m^o = \delta_{shear}^o$ for $\delta_3 = 0$ (or when $\beta \rightarrow \infty$, Shear Mode).

Delamination propagation prediction The criteria used to predict delamination propagation under mixed-mode loading conditions are usually established in terms of the energy release rates and fracture toughness. There are established test methods to obtain the Mode I and II interlaminar fracture toughness. The Double Cantilever Beam Specimen (DCB) is used for Mode I. The End Notched Flexure (ENF) or the End Loaded Split (ELS) specimens are used for Mode II. For mixed-mode I and II, the Mixed-Mode Bending (MMB) test specimen is normally used. However, further research is required to assess the Mode III interlaminar fracture toughness, G_{III} . Although some test methods have been suggested for the measurement of Mode III interlaminar fracture toughness, such as the Edge Crack Torsion [39] (ECT), there are important issues that need clarification, such as the determination of the transverse shear modulus G_{23} , which is a parameter required for the analysis [14]. Furthermore, there is no reliable mixed-mode delamination failure criterion incorporating Mode III because there is no mixed-mode test method available incorporating Mode III loading. Therefore, most of the failure criteria proposed for delamination growth were established for mixed-mode I and II loading only. For these reasons, and following Li's work [4], [5], the concept of energy release rate related with shear loading, $G_{shear} = G_{II} + G_{III}$, is used here.

For mixed-mode loading the dependence of the fracture toughness on mode ratio must be accounted for in the formulation of decohesion elements. The relation between the mixed-mode interlaminar fracture toughness and the fracture surfaces of unidirectional laminates has been thoroughly examined using scanning electron

microscope analyses [21], [40]: for epoxy composites under pure Mode I loading the fracture surface is flat indicating cleavage fractures, whereas under pure Mode II loading the fracture surface exhibit hackles having an orientation of approximately 45° with respect to the fiber direction. Under mixed-mode I and II the mechanisms are more complex, including both cleavage paths and hackles [21], [40].

The most widely used criterion to predict delamination propagation under mixed-mode loading, the *power law criterion*, is established in terms of an interaction between the energy release rates [41]:

$$\left(\frac{G_I}{G_{IC}}\right)^\alpha + \left(\frac{G_{II}}{G_{IIC}}\right)^\alpha = 1 \quad (34)$$

Reeder [21] performed mixed-mode bending (MMB) tests to measure the mixed-mode I and II interlaminar fracture toughness of composites, and obtained valuable experimental data to assess the several criteria proposed to predict delamination growth. The power law criterion obtained from (34) with $\alpha = 1$ was found to be suited to predict failure of thermoplastic PEEK matrix composites because the results were comparable to the more sophisticated criteria, while using fewer independent variables. However, the power law criterion failed to accurately capture the dependence of the mixed-mode fracture toughness on the mode ratio occurring in epoxy composites using both $\alpha = 1$ and $\alpha = 2$.

In order to accurately account for the variation of fracture toughness as a function of mode ratio in epoxy composites, the mixed-mode criterion proposed by Benzeggagh and Kenane [40] is used here (*B-K criterion*). This criterion is expressed as a function of the Mode I and Mode II fracture toughness and a parameter η obtained from MMB tests at different mode ratios:

$$G_{IC} + (G_{IIC} - G_{IC}) \left(\frac{G_{II}}{G_T}\right)^\eta = G_C, \text{ with } G_T = G_I + G_{II} \quad (35)$$

If Mode III loading occurs the criterion is:

$$G_{IC} + (G_{IIC} - G_{IC}) \left(\frac{G_{shear}}{G_T}\right)^\eta = G_C, \text{ with } G_T = G_I + G_{shear} \quad (36)$$

Figure 3 shows the predictions of the power law and B-K criteria for composites using a tough epoxy resin (IM7/977-2), a brittle epoxy resin (AS4/3501-6), and a thermoplastic resin (AS4/PEEK). The figure also includes the average of the experimental results obtained at different mode ratios (discrete points shown in Figure 3) and the α and η values used for each material.

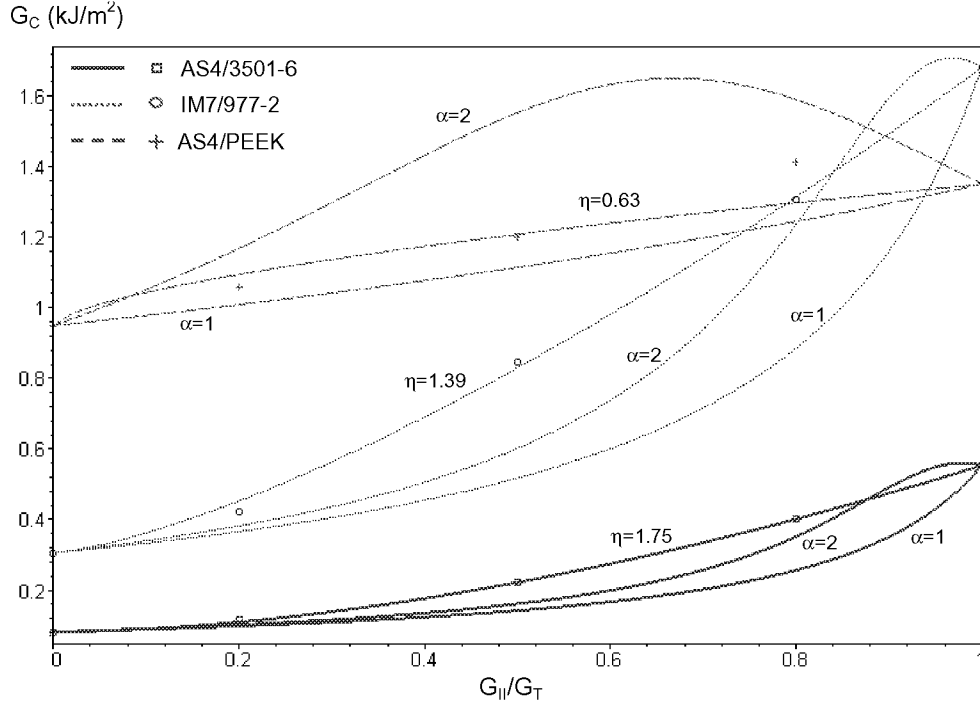


Figure 3: Mixed-mode fracture toughness

By using three parameters, G_{IC} , G_{IIC} and η , the B-K criterion represents the mixed-mode fracture toughness over a comprehensive range of mode mixity, whereas the two-parameter power law criterion that is usually implemented in decohesion elements can lead to inaccurate results over a large range of mode ratios. Furthermore, using the power law criteria with $\alpha = 2$ in epoxy based composites, values of mixed-mode fracture toughness higher than G_{IIC} occur in the interval $0.9 \leq G_{II}/G_T < 1.0$. Experimental evidence (Figure 3) shows that the maximum mixed-mode fracture toughness occurs for $G_{II}/G_T = 1$, i.e., $G_C^{\max} = G_{IIC}$. Therefore, using of the power law criterion with $\alpha = 2$ in epoxy based composites can lead to unconservative predictions in a small range of mode mixity ratios.

Figure 3 shows that both the power law criterion using $\alpha = 1$, and the B-K criterion provide reasonable results for the prediction of the mixed-mode fracture

toughness of AS4/PEEK composites. The power law criterion with $\alpha = 2$ is clearly inadequate to predict the mixed-mode fracture toughness of AS4/PEEK composites.

Based on the above results, the use of the B-K criterion in epoxy and thermoplastic based composites is recommended. Taking into account that the maximum difference obtained by the application of the power law criterion using $\alpha = 1$ to thermoplastic composites is 11.9% (at $G_{II}/G_T = 0.8$), it is considered that the power law criterion using $\alpha = 1$ can also be used, with the advantage of having one less variable than the B-K criterion. Therefore, both the B-K and the power law criterion are implemented in the decohesion element.

The energy release rates corresponding to total decohesion are obtained from:

$$G_I = \int_0^{\delta_m^{3f}} \tau_3 d\delta_3 \quad (37)$$

$$G_{II} = \int_0^{\delta_m^{2f}} \tau_2 d\delta_2 \quad (38)$$

$$G_{III} = \int_0^{\delta_m^{1f}} \tau_1 d\delta_1 \quad (39)$$

Using (24), (28) and (32) in equations (37)-(39) and substituting in (36) or in (34) the criterion for total decohesion can be established in terms of δ_m and β . Solving the equation for δ_m , the mixed-mode displacements corresponding to total decohesion, δ_m^f , are obtained for the B-K criterion as:

$$\delta_m^f = \begin{cases} \frac{2}{K\delta_m^\sigma} \left[G_{IC} + (G_{IIC} - G_{IC}) \left(\frac{\beta^2}{1 + \beta^2} \right)^\eta \right] \Leftarrow \delta_3 > 0 \\ \sqrt{(\delta_1^f)^2 + (\delta_2^f)^2} \Leftarrow \delta_3 \leq 0 \end{cases} \quad (40)$$

and for the power law criterion as:

$$\delta_m^f = \begin{cases} \frac{2(1 + \beta^2)}{K\delta_m^\sigma} \left[\left(\frac{1}{G_{IC}} \right)^\alpha + \left(\frac{\beta^2}{G_{IIC}} \right)^\alpha \right]^{-1/\alpha} \Leftarrow \delta_3 > 0 \\ \sqrt{(\delta_1^f)^2 + (\delta_2^f)^2} \Leftarrow \delta_3 \leq 0 \end{cases} \quad (41)$$

Regardless of the criterion used, pure mode loading is a particular case of the proposed formulation, as $\delta_m^f = \delta_3^f$ for $\beta = 0$ (Mode I) and $\delta_m^f = \delta_{shear}^f$ for $\delta_3 = 0$ (or when $\beta \rightarrow \infty$, Shear Mode).

Constitutive equation for mixed-mode loading The constitutive equation for mixed-mode loading is defined by the penalty parameter K , the damage evolution function d , the mixed-mode relative displacements corresponding to damage initiation and total decohesion, δ_m^o and δ_m^f , respectively, as:

$$\tau_s = D_{sr}\delta_r, \text{ with:} \quad (42)$$

$$D_{sr} = \begin{cases} \bar{\delta}_{sr}K & \Leftarrow \delta_m^{\max} \leq \delta_m^o \\ \bar{\delta}_{sr} \left[(1-d)K + Kd\bar{\delta}_{s3}\frac{\langle -\delta_3 \rangle}{-\delta_3} \right] & \Leftarrow \delta_m^o < \delta_m^{\max} < \delta_m^f \\ \bar{\delta}_{s3}\bar{\delta}_{3r}\frac{\langle -\delta_3 \rangle}{-\delta_3}K & \Leftarrow \delta_m^{\max} \geq \delta_m^f \end{cases} \quad (43)$$

$$d = \frac{\delta_m^f(\delta_m^{\max} - \delta_m^o)}{\delta_m^{\max}(\delta_m^f - \delta_m^o)}, \quad d \in [0, 1] \quad (44)$$

It is worth noticing that Equation (43) avoids the interpenetration of the crack faces of the decohesion element for softening and fully open conditions.

In order to define the loading and unloading conditions the state variable *maximum mixed-mode relative displacement*, δ_m^{\max} , and the *loading function*, F , are defined as:

$$\delta_m^{\max} = \max \{ \delta_m^{\max}, \delta_m \} \quad (45)$$

$$F(\delta_m - \delta_m^{\max}) = \frac{\langle \delta_m - \delta_m^{\max} \rangle}{\delta_m - \delta_m^{\max}} \quad (46)$$

The mixed mode softening law presented above is a single-variable response similar to the bilinear single-mode law illustrated in Figure 2, defined by a *damage evolution law* (44), by the *maximum mixed-mode relative displacement*, (45), and by the *loading function* (46). Only one state variable, the maximum relative displacement variable δ_m^{\max} , is used to track the damage at the interface. By recording the highest value attained by δ_m , the unloading response is such as shown in Figure 2. The relative displacements for initiation and ultimate failure are functions of the mode mixity β , the material properties, and the penalty stiffness.

The mixed-mode softening law can be illustrated in a single three-dimensional map by representing Mode I on the Y-Z plane, and Shear Mode in the X-Z plane, as shown in Figure 4.

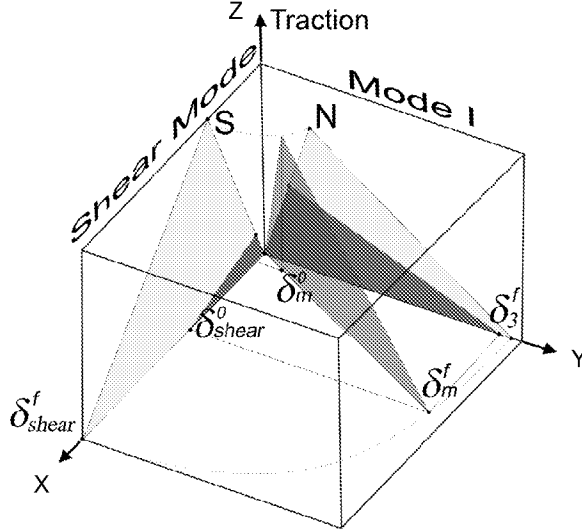


Figure 4: Mixed-mode softening law

The triangles $0 - N - \delta_3^f$ and $0 - S - \delta_{shear}^f$ are the bilinear response in Mode I and in shear mode respectively. In this three-dimensional map, any point on the 0-X-Y plane represents a mixed-mode relative displacement.

The map of all softening responses under mixed mode is illustrated in Figure 5. The curve FI represents the tractions resulting from the displacements at the onset of damage given by (33), while the curve labeled G represents the ultimate relative displacements calculated with either (40) or (41). The triangle $0 - A - B$ is the bilinear softening law for a mixed-mode relative displacement of δ_m and the triangle $0 - C - D$ in Figure 5 is the Mode I bilinear softening response. It can also be observed that the effect of compression on the material response is neglected.

2.3 Solution method for the non-linear problem

The softening nature of the decohesion element constitutive equation causes difficulties in obtaining a converged solution for the non-linear problem. Furthermore, high penalty values can lead to large unbalanced forces and shoot the iteration

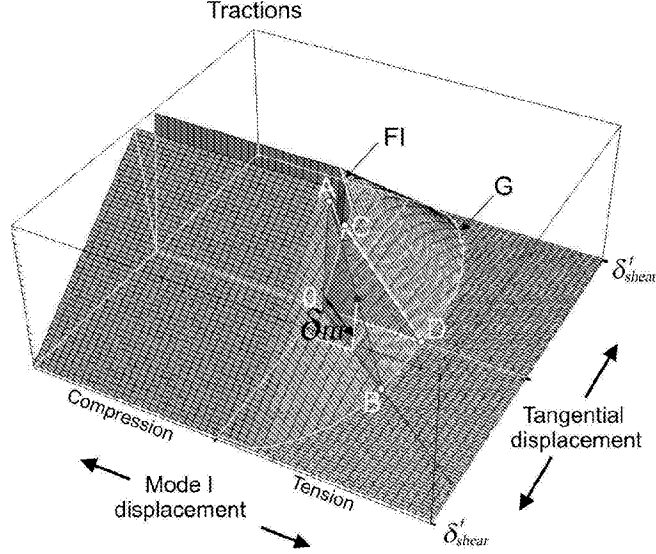


Figure 5: Map of softening response for mixed-mode delamination

process beyond its radius of convergence. Crisfield *et al.* [42] found that when using the Newton-Raphson method under load (with the arc-length method) or displacement control, the iterative solutions often failed to converge. In order to obtain convergence, a 'line search' procedure with a negative step length was proposed. Other methods such as modified cylindrical arc-length method [43] and the nodal crack opening displacement (COD) control have been proposed [22], [30].

The Newton-Raphson method under displacement control and a 'line-search' algorithm is used to solve the non-linear problem. Therefore, the *decohesion element consistent tangent stiffness operator*, must be calculated as:

$$K_{kizv}^T = \frac{\partial f_{ki}}{\partial u_{zv}} \quad (47)$$

As shown in Appendix A, the scalar components of the decohesion element

consistent tangent stiffness matrix are:

$$K_{kizv}^T = \int_{\Gamma} B_{rik} K B_{rvz} d\Gamma \Leftarrow \delta_m^{\max} \leq \delta_m^o \quad (48)$$

$$K_{kizv}^T = K_{1kizv}^T + K_{2kizv}^T \Leftarrow \delta_m^o < \delta_m^{\max} \leq \delta_m^f, \text{ where:} \quad (49)$$

$$K_{1kizv}^T = \int_{\Gamma} B_{sik} \bar{\delta}_{sr} \left[(1-d)K + K d \bar{\delta}_{s3} \frac{\langle -\delta_3 \rangle}{-\delta_3} \right] B_{rvz} d\Gamma \quad (50)$$

$$K_{2kizv}^T = - \int_{\Gamma} B_{sik} \delta_r F(\delta_m - \delta_m^{\max}) \frac{\delta_w}{\delta_m} \cdot \frac{K \delta_m^f \delta_m^o}{(\delta_m^{\max})^2 (\delta_m^f - \delta_m^o)} \Psi_{srw}(\delta_3) B_{wzv} d\Gamma \quad (51)$$

$$K_{ikzv}^T = \int_{\Gamma} B_{sik} \bar{\delta}_{s3} \bar{\delta}_{3r} \frac{\langle -\delta_3 \rangle}{-\delta_3} K B_{rvz} d\Gamma \Leftarrow \delta_m^{\max} > \delta_m^f \quad (52)$$

where i, v are global degrees of freedom, k, z represent node numbers and r, w are related with the scalar components of the relative displacements.

The function $\Psi_{srw}(\delta_3)$ is defined as:

$$\Psi_{srw}(\delta_3) = \bar{\delta}_{sr} \left(1 - \bar{\delta}_{s3} \frac{\langle -\delta_3 \rangle}{-\delta_3} \right) \left(1 - \bar{\delta}_{3w} + \frac{\langle \delta_3 \rangle}{\delta_3} \bar{\delta}_{3w} \right) \quad (53)$$

The sum in (49) is a correction of the secant stiffness, K_{1kizv}^T , due to the damage growth occurring when $F(\delta_m - \delta_m^{\max}) = 1$. Under unloading conditions, $F(\delta_m - \delta_m^{\max}) = 0$, and $K_{kizv}^T = K_{1kizv}^T$. It is worth noticing that the material tangent stiffness matrix included in K_{kizv}^T under single-mode unloading conditions corresponds to the secant stiffness shown in Figure 2, $(1-d)K$.

3 Simulation of delamination in fiber-reinforced composites

The decohesion element proposed here was implemented in the ABAQUS Finite Element code [44] as a user-written element subroutine (UEL). To verify the element under different loading conditions, the double cantilever beam (DCB) test, the end notched flexure (ENF) test, and mixed-mode bending (MMB) tests are

simulated. The numerical predictions are compared with experimental data. The DCB test consists of pure Mode I delamination. The ENF tests measure pure Mode II interlaminar fracture toughness, and the MMB delaminates under Mixed Mode I and II. In the absence of Mode III loading, $G_{shear} = G_{II}$. To investigate the accuracy of the formulation in the simulation of delamination in different materials, the DCB test is simulated for T300/977-2, a thermoset composite material, while the DCB, ENF and MMB simulations are conducted for PEEK/APC2, a thermoplastic matrix composite material.

3.1 Mode I delamination growth for an epoxy composite

The ASTM standard specimen used to determine the interlaminar fracture toughness in Mode I (G_{IC}) is the double-cantilever beam (DCB) specimen [45] represented in Figure 2 b).

A DCB test specimen of a $(0^\circ)_{24}$, T300/977-2 carbon fiber-reinforced epoxy laminate, containing a thin insert at the mid-plane near the loaded end, is simulated. This specimen is 150-mm-long, 20 mm-wide, with two 1.98-mm-thick plies, and with an initial crack length of 55 mm. The DCB tests on this specimen were performed by Morais *et al.* and reported in [46]. The material properties are shown in Table 1.

Table 1: Properties for T300/977-2 CFRP

E_{11}	$E_{22} = E_{33}$	$G_{12} = G_{13}$	G_{23}
150.0 <i>GPa</i>	11.0 <i>GPa</i>	6.0 <i>GPa</i>	3.7 <i>GPa</i>
$\nu_{12} = \nu_{13}$	ν_{23}	G_{IC}	T
0.25	0.45	0.268 <i>kJ/m²</i>	45 <i>MPa</i>

In order to define the element constitutive equation, the penalty parameter and the interlaminar tensile and shear strengths must be determined. The choice of the penalty parameter can have an effect on the solution. Too low of a value leads to an inaccurate representation of the mechanical behavior of the interface, whereas high values can promote numerical errors related to computer precision. The optimum value for the penalty parameter is the largest value that does not lead to numerical problems. Some methodologies have been proposed to define the most adequate value for penalty parameters [47]. Based on previous investigations [36], a penalty $K = 10^6$ *N/mm* is used here.

Twenty-one node solid elements are used to simulate the DCB arms, and 18-node decohesion elements with a length of 1 mm are used along the interface.

Figure 6 shows the results of 3 sets of experimental data and the numerical predictions.

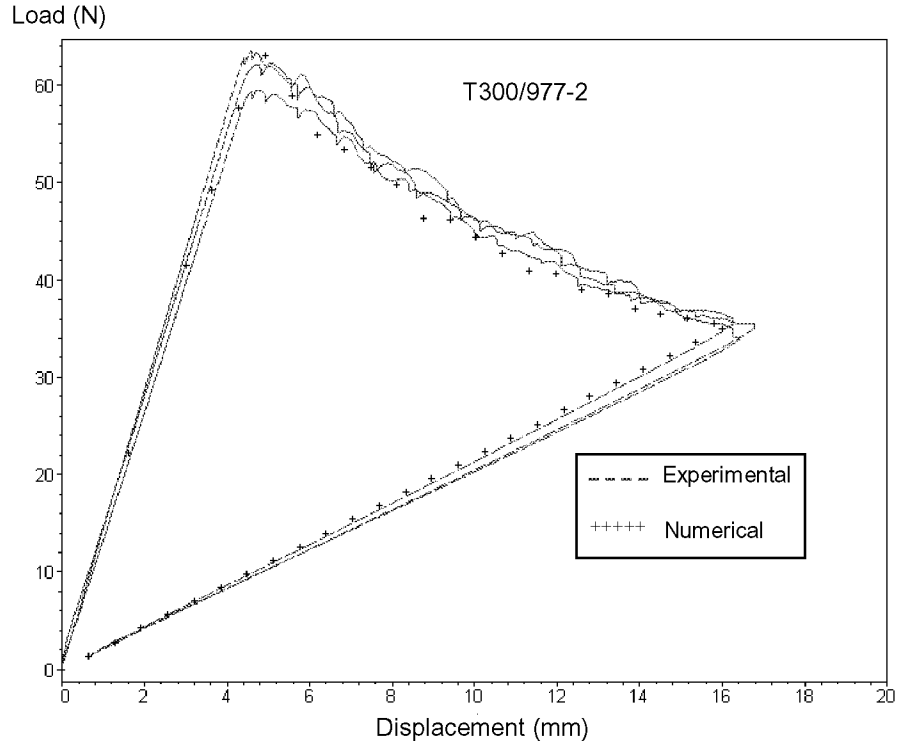


Figure 6: Experimental and numerical results for T300/977-2 CFRP

It can be seen that an excellent agreement between the experimental data and the numerical predictions is obtained. The averaged maximum load obtained in the experiments is 62.52 N, whereas the maximum load predicted is 63.11 N. The unloading response is well reproduced by the numerical model, validating the unloading behavior of the constitutive equation proposed.

3.2 Mode I, Mode II and Mixed-Mode I and II delamination growth for a PEEK composite

The most widely used specimen for mixed-mode fracture is the mixed-mode bending (MMB) specimen shown in Figure 7, which was proposed by Reeder and Crews [48], [49] and later re-designed to minimize geometric nonlinearities [50]. This test method was recently standardized by the American Society for Testing and Materials [51].

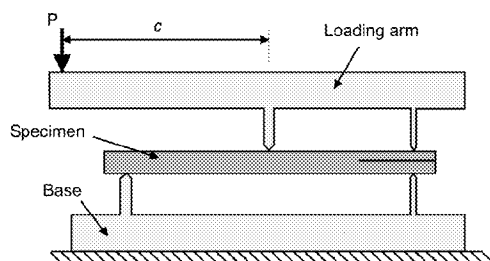


Figure 7: MMB test specimen

The main advantages of the MMB test method are the possibility of using virtually the same specimen configuration as for Mode I tests, and the capability of obtaining different mixed mode ratios, ranging from pure Mode I to pure Mode II, by changing the length c of the loading lever shown in Figure 7.

The 8-node decohesion element developed is used to simulate DCB, ENF and MMB tests in unidirectional AS4/PEEK carbon-fiber reinforced composite. The specimens simulated are 102-mm-long, 25.4 mm-wide, with two 1.56-mm-thick arms. The material properties are shown in Table 2, and a penalty stiffness $K = 10^6 N/mm$ is used.

Table 2: Properties for PEEK/APC2

E_{11}	$E_{22} = E_{33}$	$G_{12} = G_{13}$	G_{23}	$\nu_{12} = \nu_{13}$
122.7 <i>GPa</i>	10.1 <i>GPa</i>	5.5 <i>GPa</i>	3.7 <i>GPa</i>	0.25
ν_{23}	G_{IC}	G_{IIC}	T	S
0.45	0.969 <i>kJ/m²</i>	1.719 <i>kJ/m²</i>	80 <i>MPa</i>	100 <i>MPa</i>

The experimental tests were performed at different G_{II}/G_T ratios, ranging from pure Mode I loading to pure Mode II loading. The initial delamination length of the specimens (a_0) and the Mixed-Mode fracture toughness obtained experimentally are shown in Table 3.

Table 3: Experimental data

G_{II}/G_T	0% (<i>DCB</i>)	20%	50%	80%	100% (<i>ENF</i>)
G_C (<i>kJ/m²</i>)	0.969	1.103	1.131	1.376	1.719
a_o (<i>mm</i>)	32.9	33.7	34.1	31.4	39.3

Models using 150 decohesion elements along the length of the specimens, and 4 decohesion elements along the width, are created to simulate the ENF and MMB test cases. The initial size of the delamination is simulated by placing open decohesion elements along the length corresponding to the initial delamination of each specimen (see Table 3). These elements are capable of dealing with the contact conditions occurring for Mode II or Mixed-Mode I and II loading, therefore avoiding interpenetration of the delamination faces. The model of the DCB test specimen uses 102 decohesion elements along the length of the specimen.

The different G_{II}/G_T ratios are simulated by applying different loads at the middle and at the end of the test specimen. The determination of the middle and end loads for each mode ratio is presented in Appendix B. The experimental results relate the load to the displacement of the point of application of the load P in the lever (*load-point displacement*, Figure 7). Since the lever is not simulated, it is necessary to determine the load-point displacement from the displacement at the end and at the middle of the specimen, using the procedure described in Appendix C.

The B-K parameter $\eta = 2.284$ is calculated by applying the least-squares fit procedure proposed in Appendix D to the experimental data shown in Table 3.

Figure 8 shows the numerical predictions and the experimental data for all the test cases simulated, and Table 4 shows the comparison between the predicted and experimentally determined maximum loads.

Table 4: Experimental and numerical maximum loads

G_{II}/G_T	P_{\max} (experimental, N)	P_{\max} (predicted, N)	error (%)
0% (<i>DCB</i>)	147.11	153.27	-4.2
20%	108.09	86.95	19.6
50%	275.35	236.60	14.1
80%	518.66	479.86	7.5
100% (<i>ENF</i>)	733.96	695.94	5.2

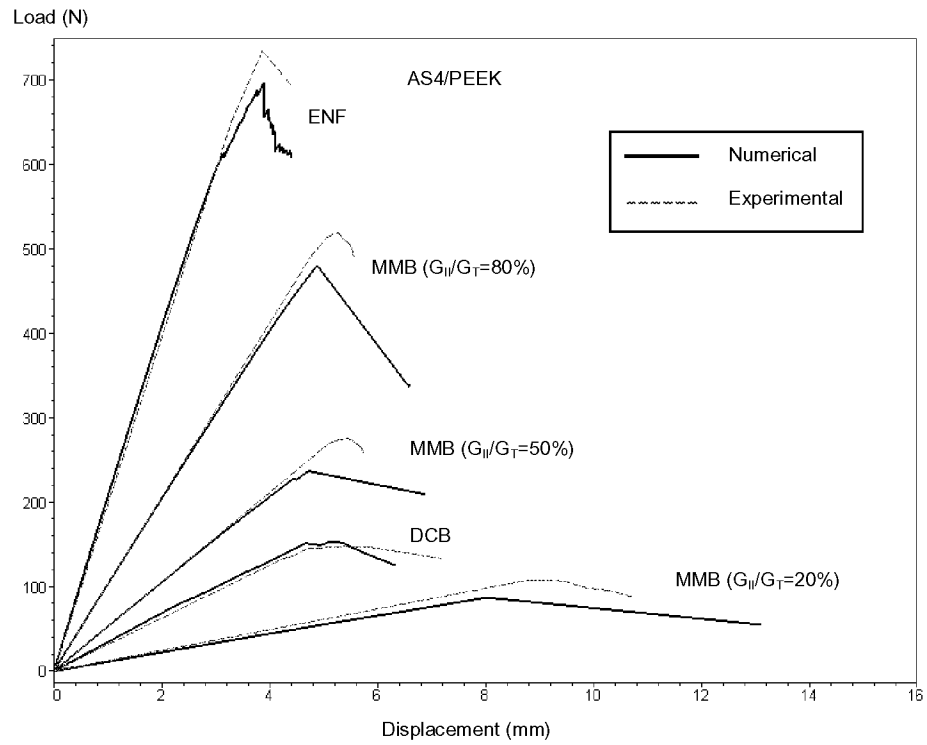


Figure 8: Predicted and experimental load-displacement relation for the different mode ratios

It can be concluded that a good agreement between the numerical predictions and the experimental results is obtained. The largest difference (19.6%) corresponds to the case of an MMB test specimen with $G_{II}/G_T = 20\%$. This fact is not surprising, since the largest difference between the fracture toughness experimentally measured and the one predicted using the B-K criterion occurs for $G_{II}/G_T = 20\%$ (see Appendix D).

4 Conclusions

A method for the simulation of progressive delamination based on decohesion elements was presented. Decohesion elements are placed between layers of solid elements that open in response to the loading situation. The onset of damage and the growth of delamination can be simulated without previous knowledge about the location, the size, or the direction of propagation of the delaminations. A softening law for mixed-mode delamination that can be applied to any interaction criterion was proposed. The criterion uses a single state variable, the maximum relative displacement, to track the damage at the interface under general loading conditions. For the linear and quadratic power law criteria, the material properties required to define the element constitutive equation are the interlaminar fracture toughnesses and the corresponding strengths. The B-K interaction law requires additionally a material parameter η that is determined from standard mixed-mode tests.

Three examples were presented that test the accuracy of the method. Simulations of the DCB and ENF test represent cases of single-mode delamination. The MMB tests that were simulated have various proportions of Mode I and Mode II loading conditions, and were simulated using a three-parameter criterion for delamination propagation. The examples analyzed are in good agreement with the test results and they indicate that the proposed mixed-mode criteria can predict the strength of composite structures that exhibit progressive delamination.

References

- [1] Camanho, P. P. and F. L. Matthews. 1999. "Delamination Onset Prediction in Mechanically Fastened Joints in Composite Laminates." *Journal of Composite Materials* 33:906-27.
- [2] Dávila, C.G. and E. R. Johnson. 1993. "Analysis of Delamination Initiation in Postbuckled Dropped-Ply Laminates." *AIAA Journal* 31 (4):721-727.
- [3] Krueger, R. and T. K. O'Brien. 2001. "A Shell/3D Modeling Technique for the Analysis of Delaminated Composite Laminates." *Composites-Part A* 32:25-44.
- [4] Li, J. and J. K. Sen. 2000. "Analysis of Frame-to-Skin Joint Pull-Off Tests and Prediction of the Delamination Failure." 42nd AIAA/ASME/ASCE/AHS/ASC Structures, Structural Dynamics and Materials Conference (Seattle, WA, U.S.A.).
- [5] Li, J. 2000. "Three-Dimensional Effects in the Prediction of Flange Delamination in Composite Skin-Stringer Pull-Off Specimens." in 15th Conference of the American Society for Composites (Texas, U.S.A.): 983-90.
- [6] Krueger, R., M. K. Cvitkovich, T. K. O'Brien, and P. J. Minguet. 2000. "Testing and Analysis of Composite Skin/Stringer Debonding Under Multi-Axial Loading." *Journal of Composite Materials* 34(15):1263-300.
- [7] Köning, M., R. Krueger, and S. Rinderknecht. 1995. "Numerical Simulation of Delamination Buckling and Growth." *Proceedings of the 10th International Conference on Composite Materials (ICCM-10)*, (Whistler, Canada).
- [8] Krueger, R. 1999. "A Shell/3D Modeling Technique for Delamination in Composite Laminates." *Proceedings of the 14th Conference of the American Society for Composites* (Ohio, U.S.A.): 843-52.
- [9] Krueger, R., P. J. Minguet, and T. K. O'Brien. 1999. "A Method for Calculating Strain Energy Release Rates in Preliminary Design of Composite Skin/Stringer Debonding Under Multi-Axial Loading". NASA TM-1999-209365.
- [10] Rybicki, E. F. and M. F. Kanninen. 1977. "A Finite Element Calculation of Stress Intensity Factors by a Modified Crack Closure Integral." *Engineering Fracture Mechanics* 9:931-38.

- [11] Rinderknecht, S. and B. Kröplin. 1994. "Calculation of Delamination Growth With Fracture and Damage Mechanics." Recent Developments in Finite Element Analysis, CIMNE, (Barcelona, Spain).
- [12] Dudgale, D. S. 1960. "Yielding of Steel Sheets Containing Slits." *Journal of Mechanics and Physics of Solids* 8:100-104.
- [13] Barenblatt, G. I. 1962. "Mathematical Theory of Equilibrium Cracks in Brittle Failure." *Advances in Applied Mechanics* 7.
- [14] Camanho, P. P., C. G. Dávila, and D. R. Ambur. 2001. "Numerical Simulation of Delamination Growth in Composite Materials." NASA-TP-211041.
- [15] de Moura, M. F., J. P. Gonçalves, A. T. Marques, and P. T. de Castro. 1997. "Modeling Compression Failure After Low Velocity Impact on Laminated Composites Using Interface Elements." *Journal of Composite Materials* 31:1462-79.
- [16] Reddy Jr., E. D., F. J. Mello, and T. R. Guess. 1997. "Modeling the Initiation and Growth of Delaminations in Composite Structures." *Journal of Composite Materials* 31:812-31.
- [17] Chen, J., M. A. Crisfield, A. J. Kinloch, E. P. Busso, F. L. Matthews, and Y. Qiu. 1999. "Predicting Progressive Delamination of Composite Material Specimens Via Interface Elements." *Mechanics of Composite Materials and Structures* 6:301-17.
- [18] Petrossian, Z. and M. R. Wisnom. 1998. "Prediction of Delamination Initiation and Growth From Discontinuous Plies Using Interface Elements." *Composites-Part A* 29:503-15.
- [19] Cui, W. and M. R. Wisnom. 1993. "A Combined Stress-Based and Fracture Mechanics-Based Model for Predicting Delamination in Composites." *Composites* 24(6):467-74.
- [20] Shahwan, K. W. and A. M. Waas. 1997. "Non-Self-Similar Decohesion Along a Finite Interface of Unilaterally Constrained Delaminations." *Proceedings of the Royal Society of London* 453:515-550.
- [21] Reeder, J. R. 1992. "An Evaluation of Mixed-Mode Delamination Failure Criteria." NASA TM 104210.

- [22] Allix, O. and A. Corigliano. 1999. "Geometrical and Interfacial Non-linearities in the Analysis of Delamination in Composites." *International Journal of Solids and Structures* 36:2189-2216.
- [23] Ahmad, S., B. M. Irons, and O. C. Zienkiewicz. 1970. "Analysis of Thick and Thin Shell Structures by Curved Finite Elements." *International Journal for Numerical Methods in Engineering* 2:419-51.
- [24] Beer, G. 1985. "An isoparametric Joint/Interface Element for Finite Element Analysis." *International Journal for Numerical Methods in Engineering* 21: 585-600.
- [25] Daudeville, L., O. Allix, and P. Ladevèze. 1995. "Delamination Analysis by Damage Mechanics: Some Applications." *Composites Engineering* 5(1):17-24.
- [26] Gonçalves, J. P., M. F. de Moura, P. T. de Castro, and A. T. Marques. 2000. "Interface Element Including Point-to-Surface Constraints for Three-Dimensional Problems With Damage Propagation." *Engineering Computations* 17(1):28-47.
- [27] Mi, Y., M. A. Crisfield, G. A. O. Davies, and H. B. Hellweg. 1998. "Progressive Delamination Using Interface Elements." *Journal of Composite Materials* 32:1246-73.
- [28] Schellekens, J. C. J. and R. de Borst. 1991. "Numerical Simulation of Free Edge Delamination in Graphite-Epoxy Laminates Under Uniaxial Tension." *Proceedings of the 6th International Conference on Composite Structures*: 647-57.
- [29] Schellekens, J. C. J. and R. de Borst. 1993. "On the Numerical Integration of Interface Elements." *International Journal for Numerical Methods in Engineering* 36:43-66.
- [30] Schellekens, J. C. J. 1992. "Computational Strategies for Composite Structures." PhD Thesis, Technical University of Delft, The Netherlands.
- [31] de Borst, R. and J. G. Rots. 1989. "Occurrence of Spurious Mechanisms in Computation of Strain-Softening Solids." *Engineering Computations* 6:272-80.

- [32] Alfano, G. and M. A. Crisfield. 2001. "Finite Element Interface Models for the Delamination Analysis of Laminated Composites: Mechanical and Computational Issues." *International Journal for Numerical Methods in Engineering* 50:1701-36.
- [33] Ungsuwarungsru, T. and W. G. Knauss. 1987. "The Role of Damage-Softened Material Behaviour in the Fracture of Composites and Adhesives." *International Journal of Fracture* 35:221-41.
- [34] Needleman, A. 1987. "A Continuum Model for Void Nucleation by Inclusion Debonding." *Journal of Applied Mechanics* 54:525-31.
- [35] Rice, J. R. 1968. "A Path Independent Integral and the Approximate Analysis of Strain Concentration by Notches and Cracks." *Journal of Applied Mechanics* 31: 379-86.
- [36] Dávila, C. G., P. P. Camanho, and M. F. Moura. 2001. "Mixed-Mode Decohesion Elements for Analyses With Progressive Delamination." 42nd AIAA/ASME/ASCE/AHS/ASC Structures, Structural Dynamics and Materials Conference (Seattle, Washington, U.S.A.).
- [37] Cui, W., M. R. Wisnom, and M. Jones. 1992. "A Comparison of Failure Criteria to Predict Delamination of Unidirectional Glass/Epoxy Specimens Waisted Through the Thickness." *Composites* 23(3):158-66.
- [38] Mohammadi, S., D. R. J. Owen, and D. Peric. 1998. "A Combined Finite/Discrete Element Algorithm for Delamination Analysis of Composites." *Finite Elements in Analysis and Design* 28:321-36.
- [39] Lee, S. M. 1993. "An Edge Crack Torsion Method for Mode III Delamination Fracture Testing." *Journal of Composites Technology & Research* 15(3):193-201.
- [40] Benzeggagh, M. L. and M. Kenane. 1996. "Measurement of Mixed-Mode Delamination Fracture Toughness of Unidirectional Glass/Epoxy Composites With Mixed-Mode Bending Apparatus." *Composites Science and Technology* 56:439-49.
- [41] Wu, E. M. and R. C. Reuter Jr. 1965. "Crack Extension in Fiberglass Reinforced Plastics." T. & AM Report No. 275, University of Illinois.

- [42] Crisfield, M. A., H. B. Hellweg, and G. A. O. Davies. 1994. "Failure Analysis of Composite Structures Using Interface Elements." Proceedings of the NAFEMS Conference on Application of Finite Elements to Composite Materials, (London, U.K.):1-4.
- [43] Hellweg, H. B. 1994. "Nonlinear Failure Simulation of Thick Composites." PhD Thesis, Imperial College of Science and Technology, University of London, U.K.
- [44] Hibbitt, Karlsson and Sorensen. 1996. ABAQUS 6.2 User's Manuals. Pawtucket, U.S.A.
- [45] Test Method D5528-01. 2002. "Standard Test Method for Mode I Interlaminar Fracture Toughness of Unidirectional Fiber-Reinforced Polymer Matrix Composites". AMERICAN SOCIETY FOR TESTING AND MATERIALS, West Conshohocken, PA, U.S.A.
- [46] Morais, A.B., Marques, A.T., and de Castro, P.T. 2000. "Estudo da Aplicação de Ensaios de Fractura Interlaminar de Modo I a Laminados Compósitos Multidireccionais," Proceedings of the 7as Jornadas de Fractura, Sociedade Portuguesa de Materiais, (Covilhã, Portugal): 90-95 (in Portuguese).
- [47] Wriggers, P., and Nour-Omid, B. 1986. "Solution Methods for Contact", Report UCB-SESM-84/09, Department of Civil Engineering, University of California, Berkeley, CA.
- [48] Crews, J. H. and J. R. Reeder. 1988. A Mixed-Mode Bending Apparatus for Delamination Testing. NASA TM 100662.
- [49] Reeder, J.R. and J.R. Crews. 1990. "Mixed-Mode Bending Method for Delamination Testing." AIAA Journal 28:1270-1276.
- [50] Reeder, J. R. and J. H. Crews. 1991. Nonlinear Analysis and Redesign of the Mixed-Mode Bending Delamination Test. NASA TM 102777.
- [51] Test Method D6671-01. 2002. "Standard Test Method for Mixed Mode I-Mode II Interlaminar Fracture Toughness of Unidirectional Fiber Reinforced Polymer Matrix Composites." AMERICAN SOCIETY FOR TESTING AND MATERIALS, West Conshohocken, PA, U.S.A.

- [52] Mi Y, Crisfield MA. "Analytical Derivation of Load/Displacement Relationship for the DCB and Proof of the FEA Formulation." 1996. Report. Department of Aeronautics, Imperial College of Science and Technology, University of London, U.K.
- [53] Reeder JR. 2000. "Refinements to the Mixed-Mode Bending Test for Delamination Toughness." Proceedings of the 15th Conference of the American Society for Composites, Texas, U.S.A.

Appendix A: Determination of the consistent tangent stiffness matrix

The tangent stiffness matrix used in solution of the non-linear problem is defined by:

$$K_{kizv}^T = \frac{\partial f_{ki}}{\partial u_{zv}} \quad (54)$$

and the decohesion element internal is load vector is:

$$f_{ki} = \int_{\Gamma} B_{sik} \tau_s d\Gamma = \int_{\Gamma} B_{sik} D_{sr} B_{rvz} d\Gamma u_{zv} \quad (55)$$

The consistent tangent stiffness matrix is obtained for the different states of the interface (no damage, softening or open interface):

Case 1 *No damage*, $\delta_m^{\max} \leq \delta_m^o$ and $D_{sr} = \bar{\delta}_{sr} K$.

From (54) and (55):

$$K_{kizv}^T = \int_{\Gamma} B_{rik} K B_{rvz} d\Gamma \quad (56)$$

Case 2 *Softening*, $\delta_m^o < \delta_m^{\max} < \delta_m^f$ and $D_{sr} = \bar{\delta}_{sr} \left[(1-d)K + K d \bar{\delta}_{s3} \frac{\langle -\delta_3 \rangle}{-\delta_3} \right]$.

From (54) and (55):

$$K_{kizv}^T = \int_{\Gamma} B_{sik} D_{sr} B_{rvz} d\Gamma + \int_{\Gamma} B_{sik} \frac{\partial D_{sr}}{\partial u_{zv}} B_{rvz} d\Gamma u_{zv} \quad (57)$$

$$K_{kizv}^T = \int_{\Gamma} B_{sik} D_{sr} B_{rvz} d\Gamma + \int_{\Gamma} B_{sik} \frac{\partial D_{sr}}{\partial u_{zv}} \delta_r d\Gamma \quad (58)$$

$$K_{kizv}^T = K_{1kizv}^T + K_{2kizv}^T \quad (59)$$

The definition of the term $\frac{\partial D_{sr}}{\partial u_{zv}}$ in K_{2kizv}^T is obtained as follows:

$$\frac{\partial D_{sr}}{\partial u_{zv}} = \frac{\partial D_{sr}}{\partial d} \frac{\partial d}{\partial u_{zv}} = -K \bar{\delta}_{sr} \left(1 - \bar{\delta}_{s3} \frac{\langle -\delta_3 \rangle}{-\delta_3} \right) \frac{\partial d}{\partial u_{zv}} = -K \Psi_{sr}^* (\delta_3) \frac{\partial d}{\partial u_{zv}} \quad (60)$$

$$\frac{\partial d}{\partial u_{zv}} = \frac{\partial d}{\partial \delta_w} \frac{\partial \delta_w}{\partial u_{zv}} = \left(\frac{\partial d}{\partial \delta_m^{\max}} \frac{\partial \delta_m^{\max}}{\partial \delta_w} \right) B_{wzv} \quad (61)$$

From (44):

$$\frac{\partial d}{\partial \delta_m^{\max}} = \frac{\delta_m^f \delta_m^o}{(\delta_m^{\max})^2 (\delta_m^f - \delta_m^o)} \quad (62)$$

From (28):

$$\frac{\partial \delta_m^{\max}}{\partial \delta_w} = F(\delta_m - \delta_m^{\max}) \frac{\delta_w}{\delta_m} \left(1 - \bar{\delta}_{3w} + \frac{\langle \delta_3 \rangle}{\delta_3} \bar{\delta}_{3w}\right) = F(\delta_m - \delta_m^{\max}) \frac{\delta_w}{\delta_m} \Psi_w^{**}(\delta_3) \quad (63)$$

Using (62) and (63) in (60):

$$\frac{\partial D_{sr}}{\partial u_{zv}} = -K \Psi_{sr}^*(\delta_3) \frac{\delta_m^f \delta_m^o}{(\delta_m^{\max})^2 (\delta_m^f - \delta_m^o)} F(\delta_m - \delta_m^{\max}) \frac{\delta_w}{\delta_m} \Psi_w^{**}(\delta_3) B_{wzv} \quad (64)$$

From (64) and (58)-(59):

$$\begin{aligned} K_{2kizv}^T &= - \int_{\Gamma} B_{sik} \delta_r F(\delta_m - \delta_m^{\max}) \frac{\delta_w}{\delta_m} \\ &\quad \cdot \frac{K \delta_m^f \delta_m^o}{(\delta_m^{\max})^2 (\delta_m^f - \delta_m^o)} \Psi_{sr}^*(\delta_3) \Psi_w^{**}(\delta_3) B_{wzv} d\Gamma \end{aligned} \quad (65)$$

$$\begin{aligned} K_{2kizv}^T &= - \int_{\Gamma} B_{sik} \delta_r F(\delta_m - \delta_m^{\max}) \frac{\delta_w}{\delta_m} \\ &\quad \cdot \frac{K \delta_m^f \delta_m^o}{(\delta_m^{\max})^2 (\delta_m^f - \delta_m^o)} \Psi_{srw}(\delta_3) B_{wzv} d\Gamma \end{aligned} \quad (66)$$

Case 3 *Open interface*, $\delta_m^{\max} \geq \delta_m^f$ and $D_{sr} = \bar{\delta}_{s3} \bar{\delta}_{3r} \frac{\langle -\delta_3 \rangle}{-\delta_3} K$.

From (54) and (55):

$$K_{kizv}^T = \int_{\Gamma} B_{sik} \bar{\delta}_{s3} \bar{\delta}_{3r} \frac{\langle -\delta_3 \rangle}{-\delta_3} K B_{rvz} d\Gamma \quad (67)$$

Appendix B: Determination of middle and end load in MMB tests

The length of the lever used in the MMB test, c , was obtained taking into account the weight of the lever. Since the lever is not simulated in the numerical models, the lengths corresponding to the different mode ratios need to be calculated.

The mode mixity ratio, κ , is defined as a function of the energy release rates as:

$$\kappa = \frac{G_{II}}{G_I + G_{II}} \cdot \frac{G_I}{G_{II}} = \frac{(1 - \kappa)}{\kappa} \quad (68)$$

The relation between Mode I and Mode II energy release rates in a MMB test specimen is [52], [49]:

$$\frac{G_I}{G_{II}} = \frac{4}{3} \left(\frac{3c - l}{c + l} \right)^2, \text{ for } c \geq \frac{l}{3} \quad (69)$$

From (68) and (69), the length of the lever can be obtained as a function of the mode mixity ratio and specimen length (l):

$$c = \frac{l \left(\frac{1}{2} \sqrt{3 \left(\frac{1-\kappa}{\kappa} \right) + 1} \right)}{3 - \frac{1}{2} \sqrt{3 \left(\frac{1-\kappa}{\kappa} \right)}} \quad (70)$$

Table 5 shows the lengths of the lever for each mode mixity use in the numerical model and in the experiments.

G_{II}/G_T	20%	50%	80%
c (numerical, <i>mm</i>)	109.4	44.4	28.4
c (experimental, <i>mm</i>)	97.4	42.2	27.6

Neglecting the weight of the lever, the middle and end loads, P_m and P_e respectively, are obtained as a function of the total load P as [49]:

$$P_m = P \left(\frac{c + l}{l} \right) \quad (71)$$

$$P_e = P \frac{c}{l} \quad (72)$$

Therefore:

$$\frac{P_m}{P_e} = \frac{c+l}{c} \quad (73)$$

From (73) and (70):

$$\frac{P_m}{P_e} = 8 \frac{6\kappa + \sqrt{3\kappa(1-\kappa)}}{3 + 9\kappa + 8\sqrt{3\kappa(1-\kappa)}} \quad (74)$$

Using (74) the relation between the load at the middle and at the end of the specimen is obtained for the different mode ratios:

Table 6: Ratio between middle and end loads

G_{II}/G_T	20%	50%	80%
P_m/P_e	1.46	2.14	2.79

The pure mode load components have been shown [49] to be given as a function of the total load applied to the specimen by:

$$P_I = P \left(\frac{3c-l}{4l} \right) \quad (75)$$

$$P_{II} = P \left(\frac{c+l}{l} \right) \quad (76)$$

From (70), (75) and (76):

$$P_I = \frac{\left(1 - \kappa + 2\sqrt{3\kappa(1-\kappa)}\right) P}{13\kappa - 1} \quad (77)$$

$$P_{II} = \frac{8 \left(6\kappa + \sqrt{3\kappa(1-\kappa)}\right) P}{3(13\kappa - 1)} \quad (78)$$

The Mode I and Mode II loads for each case are shown in Table 7.

Table 7: Mode I and Mode II load components

G_{II}/G_T	20%	50%	80%
P_I	$1.37P$	$0.41P$	$0.17P$
P_{II}	$3.15P$	$1.87P$	$1.56P$

Appendix C: Determination of the load-point displacement

The information available from the MMB test relates the load to the displacement of the load-point (Figure 7). Since the lever is not simulated in the numerical models, it is necessary to calculate the load-point displacement using the information available from the numerical models of the MMB test specimens.

The load-point displacement, Λ_{LP} , is obtained from the pure mode displacement components, Λ_I and Λ_{II} , as [53]:

$$\Lambda_{LP} = \left(\frac{3c-l}{4l} \right) \Lambda_I + \left(\frac{c+l}{l} \right) \Lambda_{II} \quad (79)$$

Using simple beam theory, Mi and Crisfield [52] calculated the Mode II displacement component, Λ_{II} , as a function of the displacement at the middle of the MMB test specimen, Λ_M :

$$\Lambda_{II} = \Lambda_M + \frac{1}{4}\Lambda_I, \text{ for } a < l \quad (80)$$

Therefore:

$$\Lambda_{LP} = \left(\frac{3c-l}{4l} \right) \Lambda_I + \left(\frac{c+l}{l} \right) \left(\Lambda_M + \frac{1}{4}\Lambda_I \right), \text{ for } a < l \quad (81)$$

The values of Λ_I and Λ_M are computed from the numerical model. The load-point displacement is then calculated using (81), being this procedure valid only for crack lengths (a) smaller than half the length of the specimen (l).

Appendix D: Experimental determination of the parameter η for the B-K delamination criterion

The problem consists in determining η from a set of experimental data using the polynomial:

$$p\left(\frac{G_{II}}{G_T}\right) = G_{IC} + (G_{IIC} - G_{IC}) \left(\frac{G_{II}}{G_T}\right)^\eta \quad (82)$$

A least-square fit is proposed. Considering the pair $\left(\left(\frac{G_{II}}{G_T}\right)_j, (G_T)_j\right)$ as the experimental data and n as the number of data points, the problem can be posed as the minimization of:

$$q = \sum_{j=1}^n \left[(G_T)_j - G_{IC} - (G_{IIC} - G_{IC}) \left(\frac{G_{II}}{G_T}\right)_j^\eta \right]^2 \quad (83)$$

Considering $\frac{dq}{d\eta} = 0$:

$$\sum_{j=1}^n \left[(G_T)_j - G_{IC} - (G_{IIC} - G_{IC}) \left(\frac{G_{II}}{G_T}\right)_j^\eta \right] \left(\frac{G_{II}}{G_T}\right)_j^\eta \ln \left(\frac{G_{II}}{G_T}\right)_j = 0 \quad (84)$$

The value of η is then obtained from the solution of equation (84). For the experimental data used (Table 3), $\eta = 2.284$. The application of the B-K criterion over the entire range of mode-mixity ratios is shown in Figure 9.

It should be noticed that only one experimental point was available for each loading condition, and that the largest difference between the B-K criterion and the experimental results occurs for $G_{II}/G_T = 0.2$.

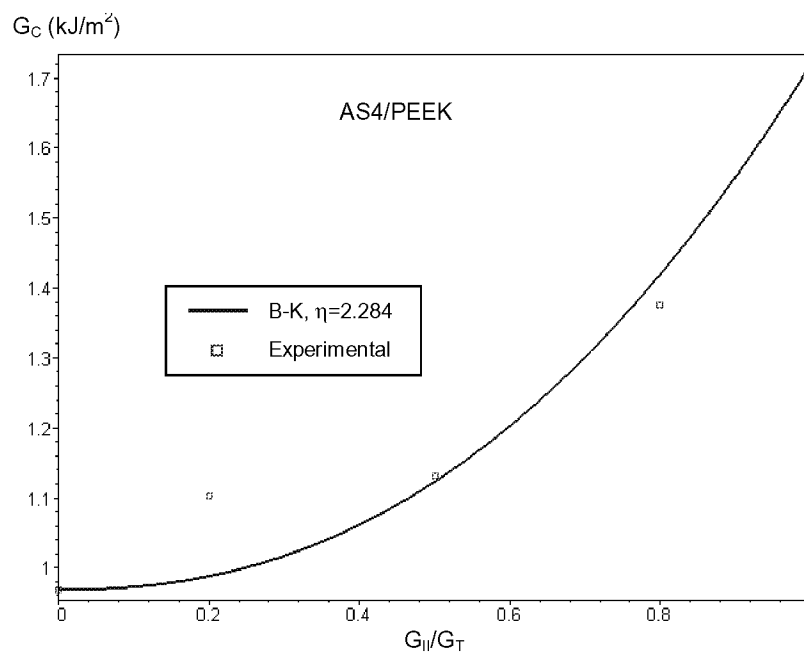


Figure 9: Prediction of BK criterion over the entire range of mode ratio.

REPORT DOCUMENTATION PAGE			Form Approved OMB No. 0704-0188
Public reporting burden for this collection of information is estimated to average 1 hour per response, including the time for reviewing instructions, searching existing data sources, gathering and maintaining the data needed, and completing and reviewing the collection of information. Send comments regarding this burden estimate or any other aspect of this collection of information, including suggestions for reducing this burden, to Washington Headquarters Services, Directorate for Information Operations and Reports, 1215 Jefferson Davis Highway, Suite 1204, Arlington, VA 22202-4302, and to the Office of Management and Budget, Paperwork Reduction Project (0704-0188), Washington, DC 20503.			
1. AGENCY USE ONLY (Leave blank)	2. REPORT DATE June 2002	3. REPORT TYPE AND DATES COVERED Technical Memorandum	
4. TITLE AND SUBTITLE Mixed-Mode Decohesion Finite Elements for the Simulation of Delamination in Composite Materials		5. FUNDING NUMBERS 706-21-21-05	
6. AUTHOR(S) Pedro P. Camanho, and Carlos G. Dávila			
7. PERFORMING ORGANIZATION NAME(S) AND ADDRESS(ES) NASA Langley Research Center Hampton, VA 23681-2199		8. PERFORMING ORGANIZATION REPORT NUMBER L-18194	
9. SPONSORING/MONITORING AGENCY NAME(S) AND ADDRESS(ES) National Aeronautics and Space Administration Washington, DC 20546-0001		10. SPONSORING/MONITORING AGENCY REPORT NUMBER NASA/TM-2002-211737	
11. SUPPLEMENTARY NOTES			
12a. DISTRIBUTION/AVAILABILITY STATEMENT Unclassified-Unlimited Subject Category 39 Distribution: Nonstandard Availability: NASA CASI (301) 621-0390		12b. DISTRIBUTION CODE	
13. ABSTRACT (Maximum 200 words) A new decohesion element with mixed-mode capability is proposed and demonstrated. The element is used at the interface between solid finite elements to model the initiation and non-self-similar growth of delaminations. A single relative displacement-based damage parameter is applied in a softening law to track the damage state of the interface and to prevent the restoration of the cohesive state during unloading. The softening law for mixed-mode delamination propagation can be applied to any mode interaction criterion such as the two-parameter power law or the three-parameter Benzeggagh-Kenane criterion. To demonstrate the accuracy of the predictions and the irreversibility capability of the constitutive law, steady-state delamination growth is simulated for quasi-static loading-unloading cycles of various single mode and mixed-mode delamination test specimens.			
14. SUBJECT TERMS Delamination; fracture mechanics; damage; decohesion elements; composite materials; finite elements		15. NUMBER OF PAGES 42	16. PRICE CODE
17. SECURITY CLASSIFICATION OF REPORT Unclassified	18. SECURITY CLASSIFICATION OF THIS PAGE Unclassified	19. SECURITY CLASSIFICATION OF ABSTRACT Unclassified	20. LIMITATION OF ABSTRACT UL